HSV-1 and influenza infection induce linear and circular splicing of the long NEAT1 isoform

Marie-Sophie Friedl[1], Lara Djakovic[2], Michael Kluge[1], Thomas Hennig[2], Adam W. Whisnant[2], Simone Backes[2], Lars Dölken[2], Caroline C. Friedel[1]*

[1] Institute of Informatics, Ludwig-Maximilians-Universität München, Amalienstr. 17, 80333 Munich, Germany

[2] Institute for Virology and Immunobiology, Julius-Maximilians-University Würzburg, Versbacher Straße 7, 97078 Würzburg, Germany

*Address correspondence to Caroline C. Friedel, caroline.friedel@bio.ifi.lmu.de

Running head: Induction of linear and circular NEAT1 splicing

Keywords: NEAT1; circRNAs; splicing; HSV-1 infection; influenza infection

Abstract

The herpes simplex virus 1 (HSV-1) virion host shut-off (*vhs*) protein cleaves both cellular and viral mRNAs but not circular RNAs (circRNAs) without an internal ribosome entry site. Here, we show that *vhs* activity leads to an accumulation of circRNAs relative to linear mRNAs during HSV-1 infection. Strikingly, we found that circular splicing of the long isoform (NEAT1_2) of the nuclear paraspeckle assembly transcript 1 (NEAT1) was massively induced during HSV-1 infection in a *vhs*-independent manner while NEAT1_2 was still bound to the chromatin. This was associated with induction of linear splicing of NEAT1_2 both within and downstream of the circRNA. NEAT1_2 splicing was absent in uninfected cells but can be induced by ectopic co-expression of the HSV-1 immediate-early proteins ICP22 and ICP27. Interestingly, NEAT1_2 circular and linear splicing was also up-regulated in influenza infection but absent in stress conditions, which disrupt transcription termination similar to but not in the same manner as HSV-1 and influenza infection. Finally, large-scale analysis of published RNA-seq data uncovered induction of NEAT1_2 splicing in cancer cells upon inhibition or knockdown of cyclin-dependent kinase 7 (CDK7) or the MED1 subunit of the Mediator complex phosphorylated by CDK7. Interestingly, CDK7 inhibition also disrupted transcription termination, highlighting a possible link between disruption of transcription termination and NEAT1_2 splicing.

Introduction

Herpes simplex virus 1 (HSV-1) is one of eight herpesviruses known to infect humans (Roizman et al. 2007). It is most commonly known for causing cold sores but can also result in life-threatening diseases. A key role in HSV-1 lytic infections is played by the virion host shut-off (*vhs*) protein, which is delivered to the infected cell by the incoming virus particles and rapidly starts cleaving both cellular and viral mRNAs (Kwong and Frenkel 1987). *Vhs* target recognition occurs during translation initiation and requires binding of *vhs* to components of the cap-binding complex eIF4F (Oroskar and Read 1989, Feng et al. 2001, Doepker et al. 2004, Sarma et al. 2008, Page and Read 2010). Notably, *vhs* is also capable of cleaving circular RNAs (circRNAs), but only if they contain an internal ribosome entry site (IRES) (Shiflett and Read 2013). CircRNAs form closed RNA-loops, in which 5' and 3' ends are covalently joined, and are naturally generated during the splicing process either by "back-splicing" of exons out of their linear order or stabilization of intron lariats (Vicens and Westhof 2014). Previously considered to occur only rarely (Nigro et al. 1991), recent large-scale RNA sequencing (RNA-seq) studies revealed the existence of thousands of circRNAs in eukaryotic cells (Salzman et al. 2012, Wilusz 2018). Due to the absence of a 5' cap or poly(A) tail and their resistance to exonucleases, circRNAs are more stable than linear RNAs (Vicens and Westhof 2014). While a function as miRNA sponge has been reported for a small number of circRNAs (Hansen et al. 2013, Memczak et al. 2013), this is now nevertheless thought to be rare (Wilusz 2018). Other functions reported for individual circRNAs involve regulation of transcription, alternative splicing and translation and some may even serve as templates for protein synthesis (Wilusz 2018). However, for most circRNAs their function remains elusive.

Recently, Shi *et al.* reported on dysregulation of circRNAs during HSV-1 infection, with 188 circRNAs being significantly up-regulated at 48 h post infection (p.i.) (Shi et al. 2018). Considering the specific targeting of *vhs* to translated mRNAs, we hypothesized that up-regulation of circRNAs may simply be a consequence of circRNAs escaping *vhs*-mediated RNA decay. We previously performed 4-thiouridine-(4sU)-tagging followed by sequencing (4sU-seq) to characterize *de novo* transcription in hourly intervals during the first 8 h of lytic HSV-1 strain 17 infection of primary human foreskin fibroblasts (HFFs) and combined this with total RNA-seq in two-hourly steps (Rutkowski et al. 2015, Hennig et al. 2018) (Supp. Fig. 1a, n=2 replicates). More recently, we applied the same experimental set-up to *Δvhs* infection to study *vhs*-dependent gene regulation (Friedel et al. 2021) (Supp. Fig. 1a). In this study, we explore these data to compare circRNA abundance between wild-type (WT) and *Δvhs* infection, confirming that circRNAs accumulated only in WT and not *Δvhs* infection.

Strikingly, this analysis also revealed *vhs*-independent induction of both a circular isoform and novel linear splicing of the long non-coding (linc)RNA nuclear paraspeckle assembly transcript 1 (NEAT1) during HSV-1 infection. The nuclear lincRNA NEAT1 is one of the most highly expressed lincRNAs and has two isoforms with identical 5' but distinct 3' ends (Sasaki et al. 2009) (Fig. 1a): A short transcript (NEAT1_1, also denoted as MENε, ~3.7nt), stabilized by a poly(A) tail and expressed in a wide range of cells (Nakagawa et al. 2011), and a long transcript (NEAT1_2, also denoted as MENβ, 22.7 nt), stabilized by a triple helical structure (Wilusz et al. 2012) but with more limited expression in particular cell types (Nakagawa et al. 2011). The HSV-1-induced circRNA is generated from the 3' region unique to the NEAT1_2 transcript (Fig. 1a). NEAT1_2 is essential for the structure of paraspeckles (Clemson et al. 2009), nuclear bodies located in the interchromatin space. NEAT1_2 forms a scaffold for

paraspeckles by being bound by a number of proteins with functions in transcription and/or RNA processing and splicing (reviewed in (Bond and Fox 2009, Prinz et al. 2019)). Paraspeckles impact gene expression by nuclear retention of adenosine-to-inosine-edited mRNAs (Prinz et al. 2019). In viral infection, NEAT1_2 plays a role in interleukin 8 (IL-8) induction by sequestering the IL-8 repressor splicing factor proline/glutamine-rich (SFPQ) to paraspeckles (Imamura et al. 2014). NEAT1 is up-regulated in HIV-1, dengue, HSV-1, Hantavirus, Hepatitis D and influenza infections (Prinz et al. 2019). Expression levels of NEAT1_2 have been shown to be positively correlated with presence of paraspeckles (Yamazaki et al. 2018) and HSV-1 infection also induces paraspeckle formation, likely through up-regulation of NEAT1 (Wang et al. 2017).

We show that combined overexpression of two HSV-1 immediate-early proteins, ICP22 and ICP27, is sufficient to induce circular and linear splicing of NEAT1_2, but neither protein alone was required nor sufficient for induction of NEAT1_2 splicing. HSV-1 and influenza infection as well as cellular stresses disrupt transcription termination, leading to read-through transcription beyond poly(A) sites for tens-of-thousands of nucleotides for many but not all cellular genes (Rutkowski et al. 2015, Hennig et al. 2018, Vilborg et al. 2015, Bauer et al. 2018, Heinz et al. 2018). Strikingly, influenza infection, but not salt and heat stress, also induces NEAT1_2 circular and linear splicing. Moreover, selective inhibition and knockdown of cyclin-dependent kinase 7 (CDK7) as well as knockdown of its phosphorylation target MED1 (Rasool et al. 2019) induce both NEAT1_2 splicing and read-through transcription in cancer cell lines. This highlights a possible link between read-through transcription and NEAT1_2 splicing and a potential role of CDK7 in HSV-1 or influenza infection.

Results

Vhs-dependent accumulation of circRNAs in HSV-1 infection

CircRNA detection from RNA-seq reads is based on identifying junction reads connecting a donor splice site of a downstream exon to the acceptor splice site of an upstream exon. Several algorithms for circRNA *de novo* detection are available, but due to high false positive rates combination of at least two algorithms is recommended (Hansen 2018). We thus employed a pipeline combining CIRI (Gao et al. 2015) and circRNA_finder (Westholm et al. 2014) (see methods) for circRNA *de novo* detection on our total RNA-seq and 4sU-seq time-courses for the first 8 h of lytic WT and *Δvhs* HSV-1 infection (Supp. Fig. 1a). This identified a total of 16,463 circRNAs in the WT time-course and 7,306 in the *Δvhs* infection time-course. Consistent with previous reports (Zhang et al. 2016) and the high stability of circRNAs, only a small number of circRNAs were detected in 4sU-RNA (119 and 194 in at least one sample of WT and *Δvhs* 4sU-seq, respectively) and the majority (>97%) was only detected in total RNA (Fig. 1b, Supp. Fig. 1b,c). Almost all of the identified circRNAs (82.6% and 92.7% for the WT and *Δvhs* infection time-courses, respectively) were already annotated in circBase, a database of circRNAs identified in large-scale RNA-seq studies (Glazar et al. 2014).

Strikingly, a substantially larger number of circRNAs was identified for WT infection in total RNA, while numbers for mock infection were comparable between time-courses and to *Δvhs* infection (Supp. Fig. 1c). Since sequencing depth influences detection of circRNAs, we correlated the number of reads mapped to the host genome to the number of detected circRNAs (Fig. 1b). This showed comparable or higher host genome coverage for total RNA-seq of *Δvhs* infection compared to WT infection. Thus, the lower number of circRNAs identified in *Δvhs* infection is not due to lower

sequencing depth. Similarly, the low numbers of circRNAs detected in 4sU-RNA are not simply due to low sequencing depth. About half (49-54%) of circRNAs identified in total RNA in mock infection were also recovered in the respective other time-course (Fig. 1c). In contrast, only 25% and 32% of circRNAs identified at 8 h p.i. WT infection were recovered in *Δvhs* and mock infection, respectively, while the majority (72-77%) of circRNAs detected in *Δvhs* and mock infection were also recovered at 8h p.i. WT infection. Thus, circRNAs are enriched at 8 h p.i. WT infection compared to both mock and *Δvhs* infection.

To evaluate abundance of individual circRNAs, circRNA read counts were normalized to the total number of reads mapping to (linear) exon-exon junctions of host protein-coding genes. We used this normalization as the fraction of (linearly) spliced reads in total RNA among all reads mapping to the human genome decreased considerably during WT infection (Supp. Fig. 1d). This is largely a consequence of HSV-1 induced read-through transcription. Read-through transcripts are rarely spliced downstream of the poly(A) site and are retained in the nucleus (Rutkowski et al. 2015, Hennig et al. 2018), thus escaping *vhs*-mediated decay. In *vhs* infection, the fraction of spliced reads did not decrease (Supp. Fig. 1e) due to reduced read-through transcription and absence of *vhs*-mediated decay of cytosolic mRNAs. Analysis of normalized circRNA counts showed that circRNAs abundances increased substantially with increasing duration of WT infection (Fig. 1d, Supp. Fig. 2a-c). By 8 h p.i. WT infection, circRNAs were enriched in total RNA by a factor of 6.5 compared to uninfected cells. In contrast, *Δvhs* infection exhibited only a very modest ~1.3-fold increase in circRNAs by 8 h p.i. (Fig. 1e, Supp. Fig. 2d-f), which can likely be attributed to the global loss of host transcriptional activity in HSV-1 infection (Spencer et al. 1997). Since circRNAs are more stable than linear RNAs, they consequently accumulate relative to linear RNAs

even in absence of *vhs*-mediated decay. Notably, if we normalize by the total numbers of reads mapped to the host, we also observe increased accumulation of circRNAs in WT infection compared to *Δvhs* infection, albeit to a lower degree (Supp. Fig. 3).

One factor that might negatively impact circRNA detection in the *Δvhs* infection time-course is the shorter read length (76nt in the *Δvhs* infection time-course vs. 101nt in the WT infection time-course, both paired-end sequencing). CIRI and circRNA_finder require that at least one read overlaps by at least 19 and 20nt, respectively, on either side of identified circular junctions. Thus, longer reads could potentially lead to identification of more circRNAs. To address this issue, we implemented an alternative approach based on aligning reads against circRNA junction sequences constructed from annotated circRNAs (see methods), which allowed to reduce the required overlap on either side of the junction to 10nt. In this case, false-positive rates are reduced by the restriction to annotated circRNAs. Results with this alignment pipeline were comparable to the original pipeline, with enrichment compared to mock being approximately the same (6.3-fold at 8 h p.i. WT infection, 1.3-fold at 8 h p.i. *Δvhs* infection; Supp. Fig. 4). This confirms the strong *vhs*-dependent accumulation of circRNAs in WT HSV-1 infection. All results reported in the following use the alignment pipeline to avoid read length biases.

We also analyzed data from a separate RNA-seq experiment in which we obtained total RNA for mock, WT, Δ*vhs* and ΔICP27 infection in the same experiment as well as subcellular fractions (chromatin-associated, nucleoplasmic and cytosolic RNA) (all 8 h p.i., n=2) (Hennig et al. 2018, Whisnant et al. 2020, Friedel et al. 2021). This revealed an accumulation of circRNAs in total RNA of both WT and ΔICP27 infection at 8 h p.i. (Supp. Fig. 5a,b), Notably, while linear regression analysis over all circRNAs estimated only an 1.5-2-fold accumulation in WT infection, some of the most highly

expressed circRNAs accumulated more strongly. Again, almost no accumulation was observed in Δ*vhs* infection (Supp. Fig. 5c). We conclude that *vhs*-mediated degradation of mRNAs leads to an accumulation of circRNAs relative to linear mRNAs during HSV-1 infection.

Induction of NEAT1 linear and circular splicing in HSV-1 infection

Strikingly, one circRNA, which was essentially absent in mock-infected cells (0-2 reads in 4sU-RNA, total RNA and all subcellular fractions, ≤0.22 normalized circRNA count), increased massively (up to >500-fold in total and 4sU-RNA) in abundance in all samples of infected cells with the notable exception of cytosolic RNA (Fig. 2, Supp. Fig. 6). This circRNA (circBase id: hsa_circ_0003812) is encoded in the unique part of the long NEAT1_2 transcript (Fig. 1a) and was also induced in ΔICP27 and *Δvhs* infection, albeit to a lesser degree. From 6 h p.i., the NEAT1_2 circRNA was among the most highly expressed circRNAs in 4sU-, total, chromatin-associated and nucleoplasmic RNA with an 80- to 538-fold enrichment in WT infection compared to mock, 7- to 21-fold enrichment in ΔICP27 infection and 11- to 108-fold enrichment in *Δvhs* infection. Some enrichment was also observed in cytosolic RNA of WT but not ΔICP27 and *Δvhs* infection, but absolute levels in cytosolic RNA remained low (Fig. 2f). This is consistent with the nuclear localization of NEAT1, which is strongly enriched in nucleoplasmic and chromatin-associated RNA but not cytosolic RNA (Hennig et al. 2018, Whisnant et al. 2020, Friedel et al. 2021). Three other NEAT1_2 circRNAs were also detected in WT total RNA, however only at very low levels.

The high abundance of the NEAT1_2 circRNA in 4sU-, nucleoplasmic and in particular chromatin-associated RNA is particularly notable, considering the small number of circRNAs that were recovered in these samples (Fig. 1b, Supp. Fig. 7). Again, sequencing depth for chromatin-associated and nucleoplasmic RNA samples was

comparable or higher than for total RNA samples from the same experiment, thus the low number of circRNAs is not an artefact of low sequencing depth. Since both nucleoplasmic and chromatin-associated RNA represent very recently transcribed RNA, the low circRNAs recovery rate in these samples and in 4sU-RNA is consistent with circRNAs being generally synthesized at very low rates. In contrast, our data indicate that the NEAT1_2 circRNA is synthesized at very high rates during infection.

Strikingly, NEAT1_2 circular splicing was accompanied by induction of linear splicing both within the circRNA region as well as downstream (Fig. 3a-b, Supp. Fig. 8-10). None of these linear splicing events were annotated, but some were already observed at low rates in uninfected cells. Normalization to the number of exon-intron reads crossing the corresponding splice acceptor and donor splice sites showed that this was not simply due to the previously reported up-regulation of NEAT1 transcription in HSV-1 infection (Imamura et al. 2014, Wang et al. 2017) (Fig. 3c). Since linear splicing was also induced downstream of the identified circRNAs (Fig. 3a,b, Supp. Fig. 8-10), linear NEAT1_2 transcripts are also spliced in HSV-1 infection. Splicing rates and enrichment compared to mock differed substantially between the different linear splice junctions within the circRNA region (Fig. 3c), indicating presence of alternative splicing isoforms of the circRNA. Induction of linear splicing was also observed in chromatin-associated, nucleoplasmic and 4sU-RNA (Fig. 3b, Supp. Fig. 9,10) and in both ΔICP27 and Δ*vhs* infection. It was less pronounced in ΔICP27 infection (Fig. 3b,c, Supp. Fig. 10), but comparable to WT infection in Δ*vhs* infection (Fig. 3c). In summary, both linear and circular splicing of NEAT1_2 is induced during HSV-1 infection while the NEAT1_2 RNA is still associated with the chromatin. Although ICP27 is not required for NEAT1_2 splicing, it may contribute.

All results shown so far were obtained in HSV-1 strain 17 infection. Recently, we also performed total RNA-seq of infection with mock, HSV-1 strain F (WT-F) and its ΔICP22 mutant at 8 and 12h p.i. (n=2) (Djakovic et al. 2021). We furthermore generated telomerase-immortalized human foreskin fibroblasts (T-HFs) that express either ICP22 in isolation (T-HFs-ICP22 cells) or in combination with ICP27 (T-HFs-ICP22/ICP27 cells) upon doxycyclin (Dox) exposure. Total RNA-seq of T-HFs-ICP22 and T-HFs-ICP22/ICP27 cells was performed both with and without Dox exposure (n=2). Strikingly, we observed that ectopic co-expression of ICP22 and ICP27 lead to induction of both circular and linear splicing of NEAT1_2 (Fig. 4a). However, ICP22 knockout did not abolish HSV-1-induced NEAT1_2 circular and linear splicing (Fig. 4a), thus ICP22 expression is not required. This also confirmed induction of linear and circular NEAT1_2 splicing in a different HSV-1 strain (Fig. 4a, Supp. Fig. 11). Although reads aligning to at least 10 nt on either side of the circular splice junction were recovered after Dox-induced expression of ICP22 alone, this was limited to 2 reads in one replicate (Fig. 4b).

To investigate whether ICP27 expression alone could induce NEAT1_2 splicing, we also analyzed our recently published 4sU-seq data of mock and HSV-1 strain KOS infection as well as ICP27 overexpression (Wang et al. 2020). This confirmed induction of both linear and circular NEAT1_2 splicing in HSV-1 KOS infection, but again only recovered one circular read in ICP27 overexpression in one replicate (Fig. 4c). In summary, our results show that neither ICP27 nor ICP22 is required for induction of linear and circular NEAT1_2 splicing but co-expression of both proteins is sufficient. Considering the small number of circular reads recovered when expressing either one of these proteins alone, we can neither confidently confirm nor exclude that either ICP22 or ICP27 alone may be sufficient to (weakly) induce NEAT1_2 circular splicing.

Influenza A infection also induces NEAT1_2 splicing

Since NEAT1_2 is also up-regulated in influenza infection (Imamura et al. 2014), we investigated presence of circRNAs in previously published total RNA-seq time-courses of influenza A/California/04/09 (H1N1), A/Wyoming/03/03 (H3N2), and A/Vietnam/1203/04 (H5N1) HALo virus infection (3, 6, 12 and 18 h p.i. plus time-matched controls) of human tracheobronchial epithelial cells (HTBE, multiplicity of infection (MOI) =5) and monocyte-derived macrophages (MDM, MOI=2) (Heinz et al. 2018). The H5N1 HALo mutant virus is an attenuated virus generated from WT influenza A/Vietnam/1203/04. H1N1 infection of HTBE cells included 24 h p.i. and two H5N1 infection time-courses of MDM cells were performed. This revealed a strong induction of NEAT1_2 circular splicing in H5N1 infection of both cell types and H3N2 infection of MDM cells as well as a weak induction in H3N2 infection of HTBE cells and H1N1 infection of MDM cells (Fig. 5a, Supp. Fig. 12). The most highly expressed circRNA was the same as for HSV-1 infection (marked by a blue bar in Fig. 5a) and its abundance increased with the duration of infection. Notably, this NEAT1_2 circRNA was also detected in some of the time-matched controls, however at significantly lower levels than in infected cells (with the exception of H1N1 infection of HTBE cells, Supp. Fig. 12a). Similar trends were observed for induction of linear splicing events, both within and downstream of the circRNA region (Fig. 5b).

It should be noted that influenza infection also induces the degradation of host RNAs via two mechanisms. Cap-snatching by the viral RNA-dependent RNA polymerase leads to cleavage of host RNAs downstream of the cap and is required for synthesis of viral mRNAs (Te Velthuis and Fodor 2016). The PA-X protein produced by all influenza A strains (Shi et al. 2012) selectively degrades RNAs transcribed by RNA Polymerase II, including long non-coding RNAs, and is localized and acts

predominantly in the nucleus (Khaperskyy et al. 2016). To exclude that induction of the NEAT1_2 circRNA is simply due to degradation of linear transcripts, we investigated overall accumulation of circRNAs in influenza infections using linear regression analysis on all circRNAs as for HSV-1 infection. This indeed showed an accumulation of circRNAs by up to 1.5-fold in H1N1 infection, 6.8-fold in H3N2 infection and 4.6-fold for H5N1 infection (Supp. Fig. 13). It also revealed induction beyond this overall accumulation for a number of other circRNAs, such as a circRNA of the ZC3HAV1 (zinc finger CCCH-type containing, antiviral 1) gene. ZC3HAV1 is induced during influenza A/WSN/33 (WSN/H1N1) infection and ectopic expression of ZC3HAV1 inhibits WSN replication (Zhang et al. 2020). Induction of the ZC3HAV1 circRNA thus likely results from the up-regulation of ZC3HAV1 transcription and associated increased circRNA biosynthesis and is not simply a consequence of host RNA degradation. We also compared fold-changes in normalized circRNA counts between infection and time-matched controls for 7077 well-expressed circRNAs (normalized circRNA count >1 in at least one condition) (Supp. Fig. 14). This showed that the hsa_circ_0003812 NEAT1_2 circRNA was among the 1% most increased circRNAs in H3N2 and H5N1 infection of MDM cells. Occasionally, it was even more up-regulated than the ZC3HAV1 circRNA. Moreover, splicing of linear NEAT1_2 transcripts, which should not escape host mRNA degradation in influenza infections, is also induced during influenza infection (Fig. 5b). Thus, our results indicate that – at least in H3N2 and H5N1 infection – induction of NEAT1_2 circular splicing is not only a consequence of influenza-induced degradation of host mRNAs.

Since both HSV-1 and influenza infection disrupt transcription termination, we also evaluated read-through for influenza infection to correlate this to the extent of induction of NEAT1_2 splicing. Paralleling NEAT1_2 induction, read-through was higher in MDM

cells than in HTBE cells and higher in H5N1 infection than in H3N2 infection (Supp. Fig. 15), while H1N1 infection led to the lowest extent of read-through. Disruption of transcription termination in influenza infection is mediated by the viral NS1 protein via inhibition of the CPSF30 subunit of the cleavage and polyadenylation specificity factor (CPSF) (Nemeroff et al. 1998). Our results are consistent with previous reports that the NS1 protein of A/California/04/09 H1N1 influenza virus cannot bind and inhibit CPSF30 (Hale et al. 2010), while NS1 of the H3N2 and H5N1 strains can (Twu et al. 2007, Das et al. 2008). Notably, however, disruption of transcription termination in influenza infection does not require the NS1-CPSF30 interaction (Bauer et al. 2018), explaining why read-through is still observed in H1N1 infection. A similar observation can be made in HSV-1 infection. Although HSV-1-induced disruption of transcription termination is mediated by ICP27 via interaction with CPSF subunits (Wang et al. 2020), reduced but significant read-through is also observed in ΔICP27 infection likely as a stress response (Vilborg et al. 2015, Hennig et al. 2018). Due to this correlation between induction of NEAT1_2 splicing and read-through, we also analyzed our previously published 4sU-seq data of 1 and 2 h salt and heat stress with regard to NEAT1_2 splicing. However, neither circular nor linear NEAT1_2 splicing was induced in either of the two stress conditions.

CDK7 inhibition induces NEAT1_2 splicing and disrupts transcription termination in cancer cell lines

To shed additional light on the molecular mechanism(s) governing NEAT1_2 splicing, we searched the *recount3* database (Wilks et al. 2021) using *Snaptron (Wilks et al. 2017)* for presence of the novel linear NEAT1_2 splicing events. *Recount3* provides read coverage data for >700,000 publicly available human and mouse RNA-seq samples from the SRA. *Snaptron* allows rapidly searching samples in *recount3* for

(linear) splice junctions within specific genomic regions. A *Snaptron* query recovered >6,000 samples in which at least one of the four most frequent NEAT1_2 linear splice junctions induced in HSV-1 infection was covered by >10 reads. This included our HSV-1 RNA-seq experiments, several other studies on HSV-1 infection, the influenza infection time-courses as well as multiple studies focusing on the identification of circRNAs. Strikingly, particular high abundance of NEAT1_2 splice junctions was found in samples of blood cells, such as platelets, erythrocytes, peripheral blood mononuclear cells (PBMCs), erythroleukemia (K562) cells, and more. Consistent with this, one of the corresponding studies reported that circRNAs are strongly enriched in platelets and erythrocytes (Alhasan et al. 2016), which both lack a cell nucleus and thus *de novo* transcription. In absence of *de novo* transcription, the high stability of circRNAs leads to their accumulation relative to linear transcripts.

Application of our circRNA alignment pipeline to two RNA-seq experiments for platelets (Kissopoulou et al. 2013) and erythrocytes (Doss et al. 2015) identified multiple NEAT1_2 circRNAs including the hsa_circ_0003812 circRNA induced by HSV-1 infection (Supp. Fig. 16). Interestingly, almost no expression was detected in the ~4 kb between the 3'end of the NEAT1_1 transcript and the 5'end of any of the circRNAs. The *de novo* circRNA finding pipeline also identified circular reads connecting the 5'end of the expressed region of NEAT1_2 to its 3'end. Thus, no linear NEAT1_2 linear transcripts were present in these cells, confirming that NEAT1_2 circRNAs are also linearly spliced. These results show that NEAT1_2 circRNAs do occur in uninfected cells, however at such low levels that they only become detectable upon degradation of linear transcripts. It should be noted that NEAT1_2 has been shown to be up-regulated in HSV-1 and influenza infection by RT-qPCR (Imamura et al. 2014), thus induction of NEAT1_2 circular splicing in HSV-1 and influenza infection cannot be

explained by loss of *de novo* transcription followed by degradation of linear transcripts. However, it partly explains the presence of NEAT1_2 circular and linear junctions in uninfected cells from the influenza infection time-courses as MDM cells were obtained from blood.

Interestingly, the *recount3* search also identified induction of NEAT1_2 linear splicing after inhibition of CDK7 by THZ1 in multiple cancer cell lines. THZ1 is a highly selective covalent inhibitor of CDK7 with anti-tumor activity against multiple different types of cancer (Li et al. 2019), but also inhibits CDK12 and CDK13 at higher concentrations (Kwiatkowski et al. 2014). Identified experiments cover prostate cancer (VCaP, LNCaP and DU145 cells) (Rasool et al. 2019), bladder cancer (HCV-29 cells) (Zarei et al. 2019), esophageal squamous cell carcinoma (TE7 and KYSE510 cells) (Jiang et al. 2017), nasopharyngeal carcinoma (C666-1, HK1 and HNE1 cells) (Yuan et al. 2017), pancreatic ductal adenocarcinoma (BxPC3, MiaPaCa-2 and PANC1 cells) (Lu et al. 2019) and chordoma (UM-Chor1 cells) (Sharifnia et al. 2019). Further literature search identified a second study of chordoma cells (UM-Chor1 and CH22) (Sheppard et al. 2021) with up to 24 h THZ1 treatment and a study on THZ1 treatment of B-cell acute lymphocytic leukemia cells (Nalm6) (Abudureheman et al. 2021). Realignment of corresponding samples confirmed linear splicing in all cell lines apart from DU145 and showed that induction increased with the duration and dosage of THZ1 treatment (Fig. 6a,b, Supp. Fig. 17a). One UM-Chor1 experiment also included actinomycin D (Act-D) treatment, which inhibits transcription but not via inhibition of cyclin-dependent kinases (CDKs) (Trask and Muller 1988). Act-D treatment, while leading to a similar relative increase in the abundance of NEAT1_2 compared to NEAT1_1 as THZ1 treatment, did not induce NEAT1_2 splicing (Supp. Fig. 17a). Thus, induction of NEAT1_2 splicing is not simply due to a general inhibition of transcription. In addition, siRNA-mediated

knockdown of CDK7 in VCaP and LNCaP cells also induced NEAT1_2 splicing (Fig. 6c). Here, many more novel splicing events were induced, even extending into the NEAT1_1 region. This indicates that indeed inhibition of CDK7, and not of other CDKs, induces NEAT1_2 splicing. Interestingly, siRNA-mediated knockdown of the MED1 component of the Mediator complex in VCaP and LNCaP cells had the same effect (Fig. 6c). CDK7 directly phosphorylates MED1 at Threonine 1457 (Rasool et al. 2019), which together with a phosphorylation at Threonine 1032 promotes MED1 association with Mediator (Belakavadi et al. 2008). This suggests that the effect of CDK7 inhibition on NEAT1_2 splicing could follow from the loss of MED1 phosphorylation and thus loss of MED1 association with Mediator.

Surprisingly, considering the previously observed strong association between linear and circular NEAT1_2 splicing, no NEAT1_2 circRNAs were recovered for any of these samples neither with our alignment-based nor our *de novo* circRNA discovery pipeline. However, in all cases almost no circRNAs (maximum 105 circRNAs, mean 18) were recovered at all, not even the most ubiquitous circRNAs such as HIPK3, CORO1C or ASXL1. As read length was ≥75 nt for all samples, this cannot be explained by short read length. It rather suggests that circRNAs were generally not or only poorly recovered in all of these studies. While a literature search identified no other studies for specific CDK7 inhibition without poly(A) selection, the *recount3* search also recovered induction of linear NEAT1_2 splicing in chromatin-associated RNA of HEK293 cells upon 2 h treatment with DRB (Werner and Ruthenburg 2015). DRB inhibits CDK7 (Yankulov et al. 1995) but also the CDK9 kinase component of the positive transcription elongation factor b (P-TEFb) (Zhu et al. 1997) and other kinases (Turinetto et al. 2009). DRB treatment indeed led to induction of the NEAT1_2 circRNA also induced by HSV-1 and influenza infection, but not any of the other NEAT1_2

circRNAs present in platelets and erythrocytes (Supp. Fig. 17b). This provides some evidence that CDK7 inhibition induces NEAT1_2 circular splicing. In any case, identification of linear splicing in absence of circRNAs confirms that the linear NEAT1_2 isoform is also spliced upon CDK7 inhibition.

Unexpectedly, we observed that CDK7 inhibition also induced read-through transcription albeit to a lesser degree than HSV-1 infection or H5N1 infection (Fig. 6d, example genes in Supp. Fig. 18). Read-through transcription after THZ1 treatment was comparable to H1N1 infection or H3N2 infection of HTBE cells, most pronounced in THZ1-treated Nalm6 cells and increased with the duration and dosage of THZ1 treatment in UM-Chor1 cells. In addition, both CDK7 and MED1 knockdown induced read-through at levels comparable to THZ1-treated Nalm6 cells. Interestingly, THZ1 treatment also resulted in extended antisense transcription at promoters, explaining the upstream transcription seen in the non-strand-specific RNA-seq for Nalm6 cells after THZ1 treatment (Supp. Fig. 18c,d). In summary, our results show that CDK7 inhibition impacts RNA transcription and processing at multiple levels.

Discussion

In this study, we report on novel circular and linear splicing of the long NEAT1_2 isoform induced in both HSV-1 and influenza infection. Linear NEAT1_2 splicing, but likely also circular splicing, is also induced upon CDK7 inhibition in cancer cell lines. Although NEAT1_2 circRNAs are abundantly observed in various blood cells in absence of *de novo* transcription, the induction of NEAT1_2 splicing in HSV-1 and influenza infection and upon CDK7 inhibition is not simply due to loss of transcriptional activity as NEAT1 is up-regulated in HSV-1 and influenza infection and transcription inhibition by Act-D does not induce NEAT1_2 splicing. Interestingly, one of the induced linear splicing events downstream of the induced circRNA was recently found to

increase extractability of NEAT1_2 from the protein phase (Chujo et al. 2017). As NEAT1_2 participates in many RNA-protein interactions in paraspeckles, its unspliced form can only be poorly extracted. Similar observations were made for other architectural RNAs (arcRNAs) of nuclear bodies. As genomic deletion of the corresponding NEAT1_2 intron did not significantly affect extractability, splicing itself appeared to be responsible for increased extractability. Chujo *et al.* concluded that NEAT1_2 as well as other arcRNAs must remain unspliced to allow formation of corresponding nuclear bodies. They hypothesized that competition by protein components of paraspeckles for binding of NEAT1_2 normally prevents association of splicing factors with NEAT1_2 and thus NEAT1_2 splicing. This raises the possibility that NEAT1_2 splicing during HSV-1 and influenza infection may simply be a by-product of up-regulation and thus increased availability of NEAT1_2 and consequently reduced competition between splicing factors and paraspeckle protein components. Alternatively, induction of NEAT1_2 splicing by unknown mechanisms might serve to counteract increased paraspeckle formation. One line of evidence arguing against NEAT1_2 splicing being a by-product of NEAT1_2 up-regulation is the absence of NEAT1_2 circular or linear splicing in heat stress as NEAT1_2 has been found to be up-regulated in the heat shock response (Lellahi et al. 2018). While the mechanism and function of induction of NEAT1_2 splicing in HSV-1 and influenza infection remain elusive, we showed that the two immediate-early HSV-1 proteins ICP22 and ICP27 were sufficient to induce NEAT1_2 circular and linear splicing. However, neither of these two proteins were required for induction of NEAT1_2 splicing and expression of either alone was not sufficient for (significant) induction of NEAT1_2 splicing.

Interestingly, we found that selective CDK7 inhibition by THZ1 not only induces NEAT1_2 splicing similar to HSV-1 and influenza infection but also disrupts

transcription termination in cancer cell lines leading to read-through transcription beyond poly(A) sites, albeit at lower levels than in HSV-1 and H5N1 influenza infection. This somewhat contradicts recent reports that 1 h THZ1 treatment suppresses RNA polymerase read-through at gene 3'ends in acute myeloid leukemia (AML) (Sampathi et al. 2019). It is, however, consistent with earlier reports of impaired 3′-end processing and termination upon CDK7 inhibition (Glover-Cutter et al. 2009, Larochelle et al. 2012). A possible explanation for this discrepancy is that more extensive CDK7 inhibition is necessary to sufficiently disrupt transcription termination as we observed significant read-through only after several hours of THZ1 treatment or CDK7 knockdown. Interestingly, CDK7 inhibition also leads to increased expression of the non-polyadenylated NEAT1_2 isoform relative to the polyadenylated NEAT1_1 isoform (Fig. 6, Supp. Fig. 17a). This was also observed in HSV-1 and influenza infection, although not consistently, and raises the possibility that read-through transcription of the NEAT1_1 poly(A) site may be involved in induction of NEAT1_2 splicing by increasing abundance of NEAT1_2. Although salt and heat stress did not induce NEAT1_2 splicing, this does not exclude a role of read-through transcription. While there are strong overlaps between the genes affected by read-through in HSV-1 infection and stress condition, there are also clear context- and condition-specific differences (Hennig et al. 2018). Furthermore, while the mechanisms leading to disruption of transcription in HSV-1 and influenza infection are now fairly well understood, they remain elusive for stress conditions. It is important to note that our analyses of NEAT1_2 splicing and read-through upon CDK7 inhibition were performed in cancer cell lines, which are particularly susceptible to CDK7 inhibition (Li et al. 2019). Dysregulation of alternative polyadenylation, often associated with wide-spread shortening of 3'UTRs, is common in cancers (Yuan et al. 2021). NEAT1 also plays different roles in cancer development and both NEAT1 isoforms have been proposed

as cancer biomarkers (Wu et al. 2015), with NEAT1_2 considered a tumor suppressor and NEAT1_1 considered to be oncogenic (Pisani and Baron 2020). Thus, read-through, relative increase of NEAT1_2 expression, or NEAT1_2 splicing could be associated with susceptibility of cancer cell lines to CDK7 inhibition.

This study identified a number of parallels between HSV-1 or influenza infection, on the one hand, and CDK7 inhibition, on the other hand. This not only includes read-through transcription and NEAT1_2 splicing, but also induction of antisense transcription upon CDK7 inhibition. We previously reported on widespread activation of antisense transcription in HSV-1 infection (Wyler et al. 2017). Moreover, widespread loss of promoter-proximal pausing was recently reported both upon CDK7 inhibition (Sampathi et al. 2019) and HSV-1 infection (Rivas et al. 2021). Previously, LDC4297A, a different selective inhibitor of CDK7, has been shown to have strong antiviral activity against HSV-1 as well as other herpesviruses (but only low efficacy against H1N1) (Hutterer et al. 2015) and CDK7 has been found to be a target of CDK inhibitors inhibiting HSV replication (Schang et al. 2002). Both studies confirm a role of CDK7 in HSV-1 infection. It is tempting to speculate that recruitment of CDK7-containing complexes, similar to recruitment of elongation factors like FACT by ICP22 (Fox et al. 2017), to the HSV-1 genome may lead to a depletion of CDK7 on host genes, thus mimicking the effects of CDK7 inhibition. In summary, our findings highlight potential important roles of NEAT1_2 splicing and CDK7 in HSV-1 and/or influenza infection.

Materials and Methods

RNA-seq data

All RNA-seq data analyzed in this study were taken from published studies and download from the NCBI sequence read archive (SRA). SRA project IDs: HSV-1 WT infection time-course: SRP044766; HSV-1 Δ*vhs* infection time-course: SRP192356;

RNA-seq of subcellular fractions: SRP110623, SRP189489, SRP191795 (same experiment but data for mutant viruses submitted separately); T-HFs-ICP22 and T-HFs-ICP22/ICP27 cells, WT strain F and ΔICP22 infection: SRP340110; WT strain KOS, ΔICP27 and ICP27 overexpression: SRP189262; influenza infection time-courses: SRP091886, SRP103821; platelets: ERP003815; erythrocytes: SRP050333; CDK7 inhibition/knockdown: VCaP, LNCaP and DU145 cells: SRP179971; HCV-29 cells: SRP217721; TE7 and KYSE510 cells: SRP068450; C666-1, HK1 and HNE1 cells: SRP101458; BxPC3, MiaPaCa-2 and PANC1 cells: SRP165924; UM-Chor1 and CH22 cells: SRP166943, SRP270819; Nalm6 cells: SRP307127; DRB treatment of HEK293 cells: SRP055770.

RNA-seq read mapping

Sequencing reads were downloaded from SRA using the sratoolkit version 2.10.8 and aligned against the human genome (GRCh37/hg19) and human rRNA sequences using ContextMap v2.7.9 (Bonfert et al. 2015) (using BWA as short read aligner (Li and Durbin 2009) and allowing a maximum indel size of 3 and at most 5 mismatches.

circRNA de novo detection

For *de novo* detection of circRNAs, we applied CIRI (Gao et al. 2015) and circRNA_finder (Westholm et al. 2014) in parallel to each sample. Both allow de novo detection of circRNAs using splice sites not annotated in the human genome. Only circRNAs were further analyzed that were detected by both algorithms. Circular reads identified by either algorithm were pooled and subsequently all reads were removed that could be mapped in a linear fashion to the genome using ContextMap. Only circRNAs with at least two supporting reads in the same sample were further analyzed.

Alignment-based circRNA detection

Candidate circular junction sequences were generated from putative spliced circRNAs sequences downloaded from circBase (Glazar et al. 2014). RNA-seq reads were aligned against circular junction sequences using BWA (Li and Durbin 2009) and reads were retained if they aligned to at least 10 nt on either side of the junction and could not be mapped in a linear fashion to the genome using ContextMap. In case of paired-end sequencing, the second read in the pair also had to align consistently within the circRNA region. circRNAs resulting from repetitive regions were discarded.

Read-through calculation

Number of read fragments per gene and in 5kb windows downstream of genes were determined from read alignments using featureCounts (Liao et al. 2014) and gene annotations from Ensembl (version 87 for GRCh37/hg19) (Zerbino et al. 2018). For strand-specific RNA-seq, the stranded mode of featureCounts was used. All fragments (read pairs for paired-end sequencing or reads for single-end sequencing) overlapping exonic regions on the corresponding strand by ≥25bp were counted for the corresponding gene. Downstream transcription for a gene was calculated as previously described (Hennig et al. 2018) as the FPKM (Fragments Per Kilobase Million) in the 5kb windows downstream of genes divided by the gene FPKM (multiplied by 100). Read-through transcription was quantified as the difference in downstream transcription between infected/treated and uninfected/control cells, with negative values set to zero.

Other analyses

Sashimi plots were generated with ggsashimi (Garrido-Martín et al. 2018). Heatmaps were generated with the heatmap.2 and pheatmap functions in R.

Supplementary Material

Supplementary Figures 1-18 are available as separate .pdf files.

Acknowledgements

This work was supported by the

Deutsche Forschungsgemeinschaft (DFG) (FR2938/10-1 to C.C.F. and LD1275/6-1 to L.D.) and by the European Research Council (ERC-2016-CoG 721016 – HERPES to L.D.). A.W.W. was the recipient of a generous grant from the Alexander von Humboldt Foundation and the German Federal Foreign Office.

References

Abudureheman T, Xia J, Li M-H, Zhou H, Zheng W-W, Zhou N, Shi R-Y, Zhu J-M, Yang L-T, Chen L, et al. 2021. CDK7 Inhibitor THZ1 Induces the Cell Apoptosis of B-Cell Acute Lymphocytic Leukemia by Perturbing Cellular Metabolism. *Frontiers in Oncology* **11**.

Alhasan A A, Izuogu O G, Al-Balool H H, Steyn J S, Evans A, Colzani M, Ghevaert C, Mountford J C, Marenah L, Elliott D J, et al. 2016. Circular RNA enrichment in platelets is a signature of transcriptome degradation. *Blood* **127**:e1-e11.

Bauer D L V, Tellier M, Martínez-Alonso M, Nojima T, Proudfoot N J, Murphy S, Fodor E. 2018. Influenza Virus Mounts a Two-Pronged Attack on Host RNA Polymerase II Transcription. *Cell Reports* **23**:2119-2129.e3.

Belakavadi M, Pandey P K, Vijayvargia R, Fondell J D. 2008. MED1 Phosphorylation Promotes Its Association with Mediator: Implications for Nuclear Receptor Signaling. *Molecular and Cellular Biology* **28**:3932-3942.

Bond C S, Fox A H. 2009. Paraspeckles: nuclear bodies built on long noncoding RNA. *The Journal of Cell Biology* **186**:637-644.

Bonfert T, Kirner E, Csaba G, Zimmer R, Friedel C C. 2015. ContextMap 2: fast and accurate context-based RNA-seq mapping. *BMC Bioinformatics* **16**:122.

Chujo T, Yamazaki T, Kawaguchi T, Kurosaka S, Takumi T, Nakagawa S, Hirose T. 2017. Unusual semi-extractability as a hallmark of nuclear body-associated architectural noncoding RNAs. *The EMBO Journal* **36**:1447-1462.

Clemson C M, Hutchinson J N, Sara S A, Ensminger A W, Fox A H, Chess A, Lawrence J B. 2009. An Architectural Role for a Nuclear Noncoding RNA: NEAT1 RNA Is Essential for the Structure of Paraspeckles. *Molecular Cell* **33**:717-726.

Das K, Ma L-C, Xiao R, Radvansky B, Aramini J, Zhao L, Marklund J, Kuo R-L, Twu K Y, Arnold E, et al. 2008. Structural basis for suppression of a host antiviral response by influenza A virus. *Proceedings of the National Academy of Sciences* **105**:13093-13098.

Djakovic L, Hennig T, Reinisch K, Milic A, Whisnant A, Wolf K, Weiß E, Haas T, Grothey A, Juerges C, et al. 2021. *Nature Portfolio*.

Doepker R C, Hsu W L, Saffran H A, Smiley J R. 2004. Herpes simplex virus virion host shutoff protein is stimulated by translation initiation factors eIF4B and eIF4H. *J Virol* **78**:4684-99.

Doss J F, Corcoran D L, Jima D D, Telen M J, Dave S S, Chi J-T. 2015. A comprehensive joint analysis of the long and short RNA transcriptomes of human erythrocytes. *BMC Genomics* **16**:952.

Feng P, Everly D N, Jr., Read G S. 2001. mRNA decay during herpesvirus infections: interaction between a putative viral nuclease and a cellular translation factor. *J Virol* **75**:10272-80.

Fox H L, Dembowski J A, DeLuca N A, Imperiale M J, Weller S, Sandri-Goldin R. 2017. A Herpesviral Immediate Early Protein Promotes Transcription Elongation of Viral Transcripts. *mBio* **8**:e00745-17.

Friedel C C, Whisnant A W, Djakovic L, Rutkowski A J, Friedl M S, Kluge M, Williamson J C, Sai S, Vidal R O, Sauer S, et al. 2021. Dissecting Herpes Simplex Virus 1-Induced Host Shutoff at the RNA Level. *J Virol* **95**.
Gao Y, Wang J, Zhao F. 2015. CIRI: an efficient and unbiased algorithm for de novo circular RNA identification. *Genome Biology* **16**:4.
Garrido-Martín D, Palumbo E, Guigó R, Breschi A. 2018. ggsashimi: Sashimi plot revised for browser- and annotation-independent splicing visualization. *PLOS Computational Biology* **14**:e1006360.
Glazar P, Papavasileiou P, Rajewsky N. 2014. circBase: a database for circular RNAs. *RNA* **20**:1666-70.
Glover-Cutter K, Larochelle S, Erickson B, Zhang C, Shokat K, Fisher R P, Bentley D L. 2009. TFIIH-Associated Cdk7 Kinase Functions in Phosphorylation of C-Terminal Domain Ser7 Residues, Promoter-Proximal Pausing, and Termination by RNA Polymerase II. *Molecular and Cellular Biology* **29**:5455-5464.
Hale B G, Steel J, Medina R A, Manicassamy B, Ye J, Hickman D, Hai R, Schmolke M, Lowen A C, Perez D R, et al. 2010. Inefficient Control of Host Gene Expression by the 2009 Pandemic H1N1 Influenza A Virus NS1 Protein. *Journal of Virology* **84**:6909-6922.
Hansen T B. 2018. Improved circRNA Identification by Combining Prediction Algorithms. *Frontiers in Cell and Developmental Biology* **6**.
Hansen T B, Jensen T I, Clausen B H, Bramsen J B, Finsen B, Damgaard C K, Kjems J. 2013. Natural RNA circles function as efficient microRNA sponges. *Nature* **495**:384.
Heinz S, Texari L, Hayes M G B, Urbanowski M, Chang M W, Givarkes N, Rialdi A, White K M, Albrecht R A, Pache L, et al. 2018. Transcription Elongation Can Affect Genome 3D Structure. *Cell* **174**:1522-1536.e22.
Hennig T, Michalski M, Rutkowski A J, Djakovic L, Whisnant A W, Friedl M S, Jha B A, Baptista M A P, L'Hernault A, Erhard F, et al. 2018. HSV-1-induced disruption of transcription termination resembles a cellular stress response but selectively increases chromatin accessibility downstream of genes. *PLoS Pathog* **14**:e1006954.
Hutterer C, Eickhoff J, Milbradt J, Korn K, Zeitträger I, Bahsi H, Wagner S, Zischinsky G, Wolf A, Degenhart C, et al. 2015. A Novel CDK7 Inhibitor of the Pyrazolotriazine Class Exerts Broad-Spectrum Antiviral Activity at Nanomolar Concentrations. *Antimicrobial Agents and Chemotherapy* **59**:2062-2071.
Imamura K, Imamachi N, Akizuki G, Kumakura M, Kawaguchi A, Nagata K, Kato A, Kawaguchi Y, Sato H, Yoneda M, et al. 2014. Long Noncoding RNA NEAT1-Dependent SFPQ Relocation from Promoter Region to Paraspeckle Mediates IL8 Expression upon Immune Stimuli. *Molecular Cell* **53**:393-406.
Jiang Y-Y, Lin D-C, Mayakonda A, Hazawa M, Ding L-W, Chien W-W, Xu L, Chen Y, Xiao J-F, Senapedis W, et al. 2017. Targeting super-enhancer-associated oncogenes in oesophageal squamous cell carcinoma. *Gut* **66**:1358-1368.
Khaperskyy D A, Schmaling S, Larkins-Ford J, McCormick C, Gaglia M M. 2016. Selective Degradation of Host RNA Polymerase II Transcripts by Influenza A Virus PA-X Host Shutoff Protein. *PLOS Pathogens* **12**:e1005427.
Kissopoulou A, Jonasson J, Lindahl T L, Osman A. 2013. Next Generation Sequencing Analysis of Human Platelet PolyA+ mRNAs and rRNA-Depleted Total RNA. *PLOS ONE* **8**:e81809.
Kwiatkowski N, Zhang T, Rahl P B, Abraham B J, Reddy J, Ficarro S B, Dastur A, Amzallag A, Ramaswamy S, Tesar B, et al. 2014. Targeting transcription regulation in cancer with a covalent CDK7 inhibitor. *Nature* **511**:616-620.
Kwong A D, Frenkel N. 1987. Herpes simplex virus-infected cells contain a function(s) that destabilizes both host and viral mRNAs. *Proc Natl Acad Sci U S A* **84**:1926-30.
Larochelle S, Amat R, Glover-Cutter K, Sansó M, Zhang C, Allen J J, Shokat K M, Bentley D L, Fisher R P. 2012. Cyclin-dependent kinase control of the initiation-to-elongation switch of RNA polymerase II. *Nature Structural & Molecular Biology* **19**:1108-1115.
Lellahi S M, Rosenlund I A, Hedberg A, Kiær L T, Mikkola I, Knutsen E, Perander M. 2018. The long noncoding RNA NEAT1 and nuclear paraspeckles are up-regulated

by the transcription factor HSF1 in the heat shock response. *Journal of Biological Chemistry* **293**:18965-18976.
Li B-B, Wang B, Zhu C-M, Tang D, Pang J, Zhao J, Sun C-H, Qiu M-J, Qian Z-R. 2019. Cyclin-dependent kinase 7 inhibitor THZ1 in cancer therapy. *Chronic Diseases and Translational Medicine* **5**:155-169.
Li H, Durbin R. 2009. Fast and accurate short read alignment with Burrows-Wheeler transform. *Bioinformatics* **25**:1754-60.
Liao Y, Smyth G K, Shi W. 2014. featureCounts: an efficient general purpose program for assigning sequence reads to genomic features. *Bioinformatics* **30**:923-30.
Lu P, Geng J, Zhang L, Wang Y, Niu N, Fang Y, Liu F, Shi J, Zhang Z-G, Sun Y-W, et al. 2019. THZ1 reveals CDK7-dependent transcriptional addictions in pancreatic cancer. *Oncogene* **38**:3932-3945.
Memczak S, Jens M, Elefsinioti A, Torti F, Krueger J, Rybak A, Maier L, Mackowiak S D, Gregersen L H, Munschauer M, et al. 2013. Circular RNAs are a large class of animal RNAs with regulatory potency. *Nature* **495**:333-8.
Nakagawa S, Naganuma T, Shioi G, Hirose T. 2011. Paraspeckles are subpopulation-specific nuclear bodies that are not essential in mice. *The Journal of Cell Biology* **193**:31-39.
Nemeroff M E, Barabino S M L, Li Y, Keller W, Krug R M. 1998. Influenza Virus NS1 Protein Interacts with the Cellular 30 kDa Subunit of CPSF and Inhibits 3′ End Formation of Cellular Pre-mRNAs. *Molecular Cell* **1**:991-1000.
Nigro J M, Cho K R, Fearon E R, Kern S E, Ruppert J M, Oliner J D, Kinzler K W, Vogelstein B. 1991. Scrambled exons. *Cell* **64**:607-613.
Oroskar A A, Read G S. 1989. Control of mRNA stability by the virion host shutoff function of herpes simplex virus. *J Virol* **63**:1897-906.
Page H G, Read G S. 2010. The virion host shutoff endonuclease (UL41) of herpes simplex virus interacts with the cellular cap-binding complex eIF4F. *J Virol* **84**:6886-90.
Pisani G, Baron B. 2020. NEAT1 and Paraspeckles in Cancer Development and Chemoresistance. *Non-Coding RNA* **6**:43.
Prinz F, Kapeller A, Pichler M, Klec C. 2019. The Implications of the Long Non-Coding RNA NEAT1 in Non-Cancerous Diseases. *International Journal of Molecular Sciences* **20**:627.
Rasool R u, Natesan R, Deng Q, Aras S, Lal P, Sander Effron S, Mitchell-Velasquez E, Posimo J M, Carskadon S, Baca S C, et al. 2019. CDK7 Inhibition Suppresses Castration-Resistant Prostate Cancer through MED1 Inactivation. *Cancer Discovery* **9**:1538-1555.
Rivas T, Goodrich J A, Kugel J F. 2021. The Herpes Simplex Virus 1 Protein ICP4 Acts as both an Activator and a Repressor of Host Genome Transcription during Infection. *Molecular and Cellular Biology* **41**:e00171-21.
Roizman B, Knipe D M, R.J. W. 2007. Herpes simplex viruses. *In Knipe D. M., Howley P. M. (ed.), Fields virology, 5th ed. Lippincott Williams & Wilkins, Philadelphia, PA.*:2501-2601.
Rutkowski A J, Erhard F, L'Hernault A, Bonfert T, Schilhabel M, Crump C, Rosenstiel P, Efstathiou S, Zimmer R, Friedel C C, et al. 2015. Widespread disruption of host transcription termination in HSV-1 infection. *Nat Commun* **6**:7126.
Salzman J, Gawad C, Wang P L, Lacayo N, Brown P O. 2012. Circular RNAs are the predominant transcript isoform from hundreds of human genes in diverse cell types. *PLoS One* **7**:e30733.
Sampathi S, Acharya P, Zhao Y, Wang J, Stengel K R, Liu Q, Savona M R, Hiebert S W. 2019. The CDK7 inhibitor THZ1 alters RNA polymerase dynamics at the 5′ and 3′ ends of genes. *Nucleic Acids Research* **47**:3921-3936.
Sarma N, Agarwal D, Shiflett L A, Read G S. 2008. Small interfering RNAs that deplete the cellular translation factor eIF4H impede mRNA degradation by the virion host shutoff protein of herpes simplex virus. *J Virol* **82**:6600-9.
Sasaki Y T F, Ideue T, Sano M, Mituyama T, Hirose T. 2009. MENε/β noncoding RNAs are essential for structural integrity of nuclear paraspeckles. *Proceedings of the National Academy of Sciences* **106**:2525-2530.

Schang L M, Bantly A, Knockaert M, Shaheen F, Meijer L, Malim M H, Gray N S, Schaffer P A. 2002. Pharmacological Cyclin-Dependent Kinase Inhibitors Inhibit Replication of Wild-Type and Drug-Resistant Strains of Herpes Simplex Virus and Human Immunodeficiency Virus Type 1 by Targeting Cellular, Not Viral, Proteins. *Journal of Virology* **76**:7874-7882.
Sharifnia T, Wawer M J, Chen T, Huang Q-Y, Weir B A, Sizemore A, Lawlor M A, Goodale A, Cowley G S, Vazquez F, et al. 2019. Small-molecule targeting of brachyury transcription factor addiction in chordoma. *Nature Medicine* **25**:292-300.
Sheppard H E, Dall'Agnese A, Park W D, Shamim M H, Dubrulle J, Johnson H L, Stossi F, Cogswell P, Sommer J, Levy J, et al. 2021. Targeted brachyury degradation disrupts a highly specific autoregulatory program controlling chordoma cell identity. *Cell Reports Medicine* **2**.
Shi J, Hu N, Mo L, Zeng Z, Sun J, Hu Y. 2018. Deep RNA Sequencing Reveals a Repertoire of Human Fibroblast Circular RNAs Associated with Cellular Responses to Herpes Simplex Virus 1 Infection. *Cellular Physiology and Biochemistry* **47**:2031-2045.
Shi M, Jagger B W, Wise H M, Digard P, Holmes E C, Taubenberger J K. 2012. Evolutionary Conservation of the PA-X Open Reading Frame in Segment 3 of Influenza A Virus. *Journal of Virology* **86**:12411-12413.
Shiflett L A, Read G S. 2013. mRNA Decay during Herpes Simplex Virus (HSV) Infections: Mutations That Affect Translation of an mRNA Influence the Sites at Which It Is Cleaved by the HSV Virion Host Shutoff (Vhs) Protein. *Journal of Virology* **87**:94-109.
Spencer C A, Dahmus M E, Rice S A. 1997. Repression of host RNA polymerase II transcription by herpes simplex virus type 1. *J Virol* **71**:2031-40.
Te Velthuis A J, Fodor E. 2016. Influenza virus RNA polymerase: insights into the mechanisms of viral RNA synthesis. *Nat Rev Microbiol* **14**:479-93.
Trask D K, Muller M T. 1988. Stabilization of type I topoisomerase-DNA covalent complexes by actinomycin D. *Proceedings of the National Academy of Sciences* **85**:1417-1421.
Turinetto V, Porcedda P, Orlando L, De Marchi M, Amoroso A, Giachino C. 2009. The cyclin-dependent kinase inhibitor 5, 6-dichloro-1-beta-D-ribofuranosylbenzimidazole induces nongenotoxic, DNA replication-independent apoptosis of normal and leukemic cells, regardless of their p53 status. *BMC Cancer* **9**:281.
Twu K Y, Kuo R-L, Marklund J, Krug R M. 2007. The H5N1 Influenza Virus NS Genes Selected after 1998 Enhance Virus Replication in Mammalian Cells. *Journal of Virology* **81**:8112-8121.
Vicens Q, Westhof E. 2014. Biogenesis of Circular RNAs. *Cell* **159**:13-14.
Vilborg A, Passarelli Maria C, Yario Therese A, Tycowski Kazimierz T, Steitz Joan A. 2015. Widespread Inducible Transcription Downstream of Human Genes. *Molecular Cell* **59**:449-461.
Wang X, Hennig T, Whisnant A W, Erhard F, Prusty B K, Friedel C C, Forouzmand E, Hu W, Erber L, Chen Y, et al. 2020. Herpes simplex virus blocks host transcription termination via the bimodal activities of ICP27. *Nat Commun* **11**:293.
Wang Z, Fan P, Zhao Y, Zhang S, Lu J, Xie W, Jiang Y, Lei F, Xu N, Zhang Y. 2017. NEAT1 modulates herpes simplex virus-1 replication by regulating viral gene transcription. *Cellular and Molecular Life Sciences* **74**:1117-1131.
Werner Michael S, Ruthenburg Alexander J. 2015. Nuclear Fractionation Reveals Thousands of Chromatin-Tethered Noncoding RNAs Adjacent to Active Genes. *Cell Reports* **12**:1089-1098.
Westholm Jakub O, Miura P, Olson S, Shenker S, Joseph B, Sanfilippo P, Celniker Susan E, Graveley Brenton R, Lai Eric C. 2014. Genome-wide Analysis of Drosophila Circular RNAs Reveals Their Structural and Sequence Properties and Age-Dependent Neural Accumulation. *Cell Reports* **9**:1966-1980.
Whisnant A W, Jurges C S, Hennig T, Wyler E, Prusty B, Rutkowski A J, L'Hernault A, Djakovic L, Gobel M, Doring K, et al. 2020. Integrative functional genomics decodes herpes simplex virus 1. *Nat Commun* **11**:2038.
Wilks C, Gaddipati P, Nellore A, Langmead B. 2017. Snaptron: querying splicing patterns across tens of thousands of RNA-seq samples. *Bioinformatics* **34**:114-116.

Wilks C, Zheng S C, Chen F Y, Charles R, Solomon B, Ling J P, Imada E L, Zhang D, Joseph L, Leek J T, et al. 2021. recount3: summaries and queries for large-scale RNA-seq expression and splicing. *bioRxiv*:2021.05.21.445138.
Wilusz J E. 2018. A 360° view of circular RNAs: From biogenesis to functions. *Wiley Interdisciplinary Reviews: RNA* **9**:e1478.
Wilusz J E, JnBaptiste C K, Lu L Y, Kuhn C-D, Joshua-Tor L, Sharp P A. 2012. A triple helix stabilizes the 3′ ends of long noncoding RNAs that lack poly(A) tails. *Genes & Development* **26**:2392-2407.
Wu Y, Yang L, Zhao J, Li C, Nie J, Liu F, Zhuo C, Zheng Y, Li B, Wang Z, et al. 2015. Nuclear-enriched abundant transcript 1 as a diagnostic and prognostic biomarker in colorectal cancer. *Molecular Cancer* **14**:191.
Wyler E, Menegatti J, Franke V, Kocks C, Boltengagen A, Hennig T, Theil K, Rutkowski A, Ferrai C, Baer L, et al. 2017. Widespread activation of antisense transcription of the host genome during herpes simplex virus 1 infection. *Genome Biology* **18**:209.
Yamazaki T, Souquere S, Chujo T, Kobelke S, Chong Y S, Fox A H, Bond C S, Nakagawa S, Pierron G, Hirose T. 2018. Functional Domains of NEAT1 Architectural lncRNA Induce Paraspeckle Assembly through Phase Separation. *Molecular Cell* **70**:1038-1053.e7.
Yankulov K, Yamashita K, Roy R, Egly J-M, Bentley D L. 1995. The Transcriptional Elongation Inhibitor 5,6-Dichloro-1-β-D-ribofuranosylbenzimidazole Inhibits Transcription Factor IIH-associated Protein Kinase (∗). *Journal of Biological Chemistry* **270**:23922-23925.
Yuan F, Hankey W, Wagner E J, Li W, Wang Q. 2021. Alternative polyadenylation of mRNA and its role in cancer. *Genes & Diseases* **8**:61-72.
Yuan J, Jiang Y-Y, Mayakonda A, Huang M, Ding L-W, Lin H, Yu F, Lu Y, Loh T K S, Chow M, et al. 2017. Super-Enhancers Promote Transcriptional Dysregulation in Nasopharyngeal Carcinoma. *Cancer Research* **77**:6614-6626.
Zarei M, Du H, Nassar A H, Yan R E, Giannikou K, Johnson S H, Lam H C, Henske E P, Wang Y, Zhang T, et al. 2019. Tumors with TSC mutations are sensitive to CDK7 inhibition through NRF2 and glutathione depletion. *Journal of Experimental Medicine* **216**:2635-2652.
Zerbino D R, Achuthan P, Akanni W, Amode M R, Barrell D, Bhai J, Billis K, Cummins C, Gall A, Giron C G, et al. 2018. Ensembl 2018. *Nucleic Acids Res* **46**:D754-D761.
Zhang B, Goraya M U, Chen N, Xu L, Hong Y, Zhu M, Chen J-L. 2020. Zinc Finger CCCH-Type Antiviral Protein 1 Restricts the Viral Replication by Positively Regulating Type I Interferon Response. *Frontiers in Microbiology* **11**.
Zhang Y, Xue W, Li X, Zhang J, Chen S, Zhang J-L, Yang L, Chen L-L. 2016. The Biogenesis of Nascent Circular RNAs. *Cell Reports* **15**:611-624.
Zhu Y, Pe'ery T, Peng J, Ramanathan Y, Marshall N, Marshall T, Amendt B, Mathews M B, Price D H. 1997. Transcription elongation factor P-TEFb is required for HIV-1 Tat transactivation in vitro. *Genes & Development* **11**:2622-2632.

Figure legends:

Fig. 1: *vhs*-dependent accumulation of circRNAs in HSV-1 infection

(a) Genomic coordinates of the NEAT1_1 (polyadenylated) and NEAT1_2 (non-polyadenylated) transcript (blue) and the circRNA induced in HSV-1 and influenza infection (red). **(b)** Scatterplot comparing the number of reads mapped to the human genome against the number of distinct circular splice sites identified by *de novo*

circRNA detection for the total RNA and 4sU-RNA time-courses in HSV-1 WT and Δ*vhs* infection. Numbers are shown separately for each replicate. **(c)** Venn diagram comparing the number of identified circRNAs in at least one replicate of total RNA between uninfected samples of the WT and Δ*vhs* infection time-courses (top), between 8 h p.i. in WT and Δ*vhs* infection (middle) and 8 h p.i. and uninfected samples of the WT infection time-course (bottom). **(d,e)** Scatterplots comparing normalized circRNA counts (normalized to the number of linear junction reads mapped to the host genome) between mock and 8 h p.i. WT infection **(d)** and mock and 8 h p.i. Δ*vhs* infection **(e)**. Linear regression analysis was used to estimate the accumulation of circRNAs compared to mock infection. Corresponding scatterplots for 2, 4 and 6 h p.i. are shown in Sup. Fig. 2.

Fig. 2: Induction of a NEAT1_2 circRNA in WT, Δ*vhs* and ΔICP27 infection

Induction of a NEAT1_2 circRNA (hsa_circ_0003812) in 4sU- **(a,d)**, total **(b,e)** and chromatin-associated RNA **(c)** in WT **(a-c)**, Δ*vhs* **(c-f)** and ΔICP27 infection **(c,f)**. Enrichment (:=ε) compared to mock infection was calculated as the ratio of normalized circRNA counts between uninfected and infected cells using a pseudocount of 0.1 to avoid division by zero. Numbers on top of each figure indicate the number of circRNAs identified in the corresponding condition with a higher normalized circRNA count (=:n_h) than hsa_circ_0003812. NA = no hsa_circ_0003812 junction reads were found in the corresponding condition. **(f)** hsa_circ_0003812 is observed at low levels in cytosolic RNA in WT, but not mock, Δ*vhs* and ΔICP27 infection. Results for nucleoplasmic RNA and total RNA from the subcellular fractions experiment are shown in Supp. Fig. 6.

Fig. 3: Circular NEAT1_2 splicing is associated with novel linear splicing

(a,b) Sashimi plots showing NEAT1 read coverage (overlay of both replicates) and circular (red) and linear (same color as read coverage) splice junctions as arcs connecting acceptor and donor splice site in **(a)** selected samples of the total RNA time-courses of WT and Δ*vhs* infection and **(b)** chromatin-associated RNA in WT, Δ*vhs* and ΔICP27 infection. Number of junction reads are annotated to arcs separately for the two replicates. Junctions are only shown if at least 4 reads align by at least 10 nt on both sides of the junction. Genomic coordinates of NEAT1 transcripts and the HSV-1-induced circRNA are shown at the bottom. NEAT1 is located on the positive strand. Sashimi plots of the full total RNA and 4sU-RNA time-courses and nucleoplasmic RNA and total RNA from the subcellular fractions experiment are shown in Sup. Fig. 8, 9 and 10, respectively. **(c)** Heatmap of linear splicing read counts normalized to the number of exon-intron reads crossing the corresponding acceptor and donor splice sites for the WT and Δ*vhs* infection time-courses and the subcellular fraction experiment (dark red = high, white = low, see color bar on the right). Counts include only junction and exon-intron reads overlapping by at least 10 nt of either side of the junction or exon-intron boundary, respectively. A pseudocount of 0.01 was used to avoid division by zero. Hierarchical clustering of linear splice junctions was performed using Euclidean distances and Ward's clustering criterion. Rectangles on top below the dendrogram indicate whether splicing occurs within or downstream of the hsa_circ_0003812 circRNA. Colors on the left indicate the virus and time-point of infection (light colors early in infection, dark colors 8 h p.i, cyan = WT, blue = Δ*vhs*, gold = ΔICP27).

Fig. 4: Combined overexpression of ICP22 and ICP27 is sufficient for induction of NEAT1_2 splicing

Sashimi plots as in Fig. 3 showing read coverage and circular and linear splice junctions in **(a)** T-HFs-ICP22/ICP27 cells without and with Dox-induced co-expression of ICP22 and ICP27 as well as mock, WT-F and ΔICP22 infection at 12 h p.i., **(b)** T-HFs-ICP22 cells without and with Dox-induced ICP22 expression and **(c)** mock and HSV-1 strain KOS infection as well as ICP27 over-expression. For **(b)** and **(c)** all junction reads are shown covering at least 10nt on either side of the junction, while a minimum read count of 4 was again required for **(a)**. For an explanation of sashimi plots, see caption to Fig. 3. Circular splice junctions are marked in red, linear splice junctions in the same color as read coverage.

Fig. 5: Induction of NEAT1_2 circular and linear splicing in influenza infection

(a) Heatmap of normalized circRNA counts (normalized to number of linear splice junctions mapped to the host genome) for three NEAT1_2 circRNAs in H1N1, H3N2 and H5N1 infection of HTBE and MDM cells and time-matched controls. The NEAT1_2 hsa_circ_0003812 also induced in HSV-1 infection is marked by a blue rectangle below the dendrogram. Influenza strain and time-points of infection are color-coded on the left (white=time-matched control, cyan=H1N1, green=H3N2, purple=H5N1, darker colors indicate later time-points). **(b)** Heatmap of linear splicing read counts normalized to the number of exon-intron reads crossing the corresponding acceptor and donor splice sites in influenza infection and time-matched controls (dark red = high, white = low, see color bar on the right). Counts include only junction and exon-intron reads overlapping by at least 10 nt of either side of the junction or exon-intron boundary, respectively. A pseudocount of 0.01 was used to avoid division by zero. Colors on the

left indicate time-points of infection as in **(a)**. Colored rectangles on top below the dendrogram indicate whether linear splice junctions are also observed in HSV-1 infection (cyan) or are within (blue) or downstream (gray) of the circRNAs region. Hierarchical clustering in **(a,b)** was performed using Euclidean distances and Ward's clustering criterion.

Fig. 6: Induction of NEAT1_2 splicing and read-through upon CDK7 inhibition

(b) Heatmap of linear splicing read counts normalized to the number of exon-intron reads crossing the corresponding acceptor and donor splice sites upon treatment by DMSO/control, THZ1 or Act-D or knockdown (KD) of CDK7 or MED1 (dark red = high, white = low, see color bar on the right). Counts include only junction and exon-intron reads overlapping by at least 10 nt of either side of the junction or exon-intron boundary, respectively. A pseudocount of 0.01 was used to avoid division by zero. Hierarchical clustering was performed using Euclidean distances and Ward's clustering criterion. **(b,c)** Sashimi plots as in Fig. 3 showing read coverage and linear splice junctions in UM-Chor1 cells after **(b)** 4, 8, 12 and 24 h THZ1 or control treatment (3 replicates each) and **(c)** CDK7 and MED1 knockdown in VCaP and LNCaP cells (2 replicates each). All junctions are shown that are covered by at least 4 reads aligning to at least 10 nt on either side of the junction. **(d)** Boxplots showing distribution of %read-through (for calculation see methods) after THZ1 treatment or CDK7 or MED1 knockdown in example studies.

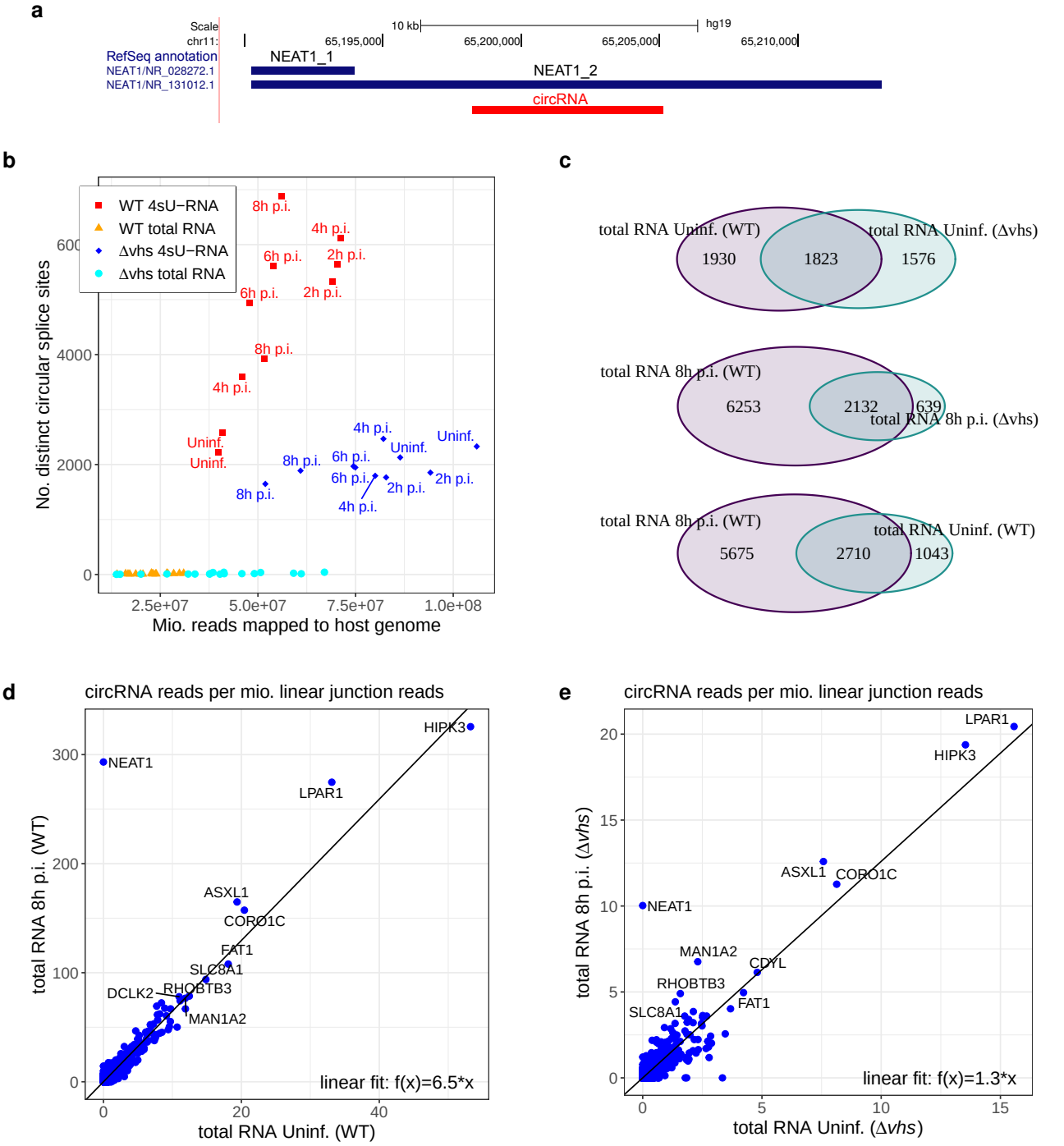
a
Scale
chr11:
10 kb
hg19
65,195,000
65,200,000
65,205,000
65,210,000
RefSeq annotation
NEAT1/NR_028272.1
NEAT1/NR_131012.1
NEAT1_1
NEAT1_2
circRNA
b
WT 4sU−RNA
WT total RNA
Δvhs 4sU−RNA
Δvhs total RNA
No. distinct circular splice sites
Mio. reads mapped to host genome
2.5e+07
5.0e+07
7.5e+07
1.0e+08
c
total RNA Uninf. (WT)
total RNA Uninf. (Δvhs)
1930
1823
1576
total RNA 8h p.i. (WT)
total RNA 8h p.i. (Δvhs)
6253
2132
639
total RNA 8h p.i. (WT)
total RNA Uninf. (WT)
5675
2710
1043
d
circRNA reads per mio. linear junction reads
total RNA 8h p.i. (WT)
total RNA Uninf. (WT)
HIPK3
NEAT1
LPAR1
ASXL1
CORO1C
FAT1
SLC8A1
DCLK2
RHOBTB3
MAN1A2
linear fit: f(x)=6.5*x
e
circRNA reads per mio. linear junction reads
total RNA 8h p.i. (Δvhs)
total RNA Uninf. (Δvhs)
LPAR1
HIPK3
ASXL1
CORO1C
NEAT1
MAN1A2
CDYL
RHOBTB3
FAT1
SLC8A1
linear fit: f(x)=1.3*x

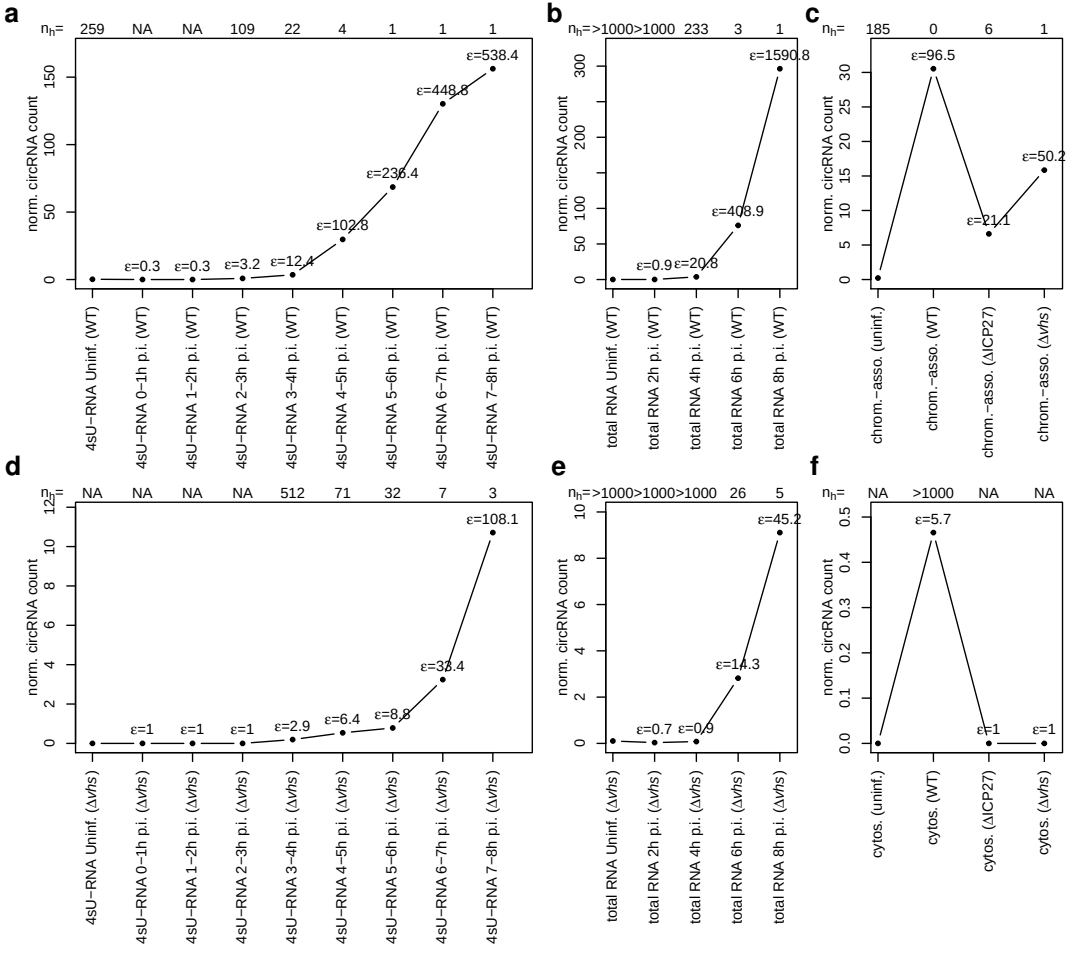
a
n_h= 259 NA NA 109 22 4 1 1 1
norm. circRNA count
ε=0.3 ε=0.3 ε=3.2 ε=12.4 ε=102.8 ε=236.4 ε=448.8 ε=538.4
4sU−RNA Uninf. (WT)
4sU−RNA 0−1h p.i. (WT)
4sU−RNA 1−2h p.i. (WT)
4sU−RNA 2−3h p.i. (WT)
4sU−RNA 3−4h p.i. (WT)
4sU−RNA 4−5h p.i. (WT)
4sU−RNA 5−6h p.i. (WT)
4sU−RNA 6−7h p.i. (WT)
4sU−RNA 7−8h p.i. (WT)
b
n_h= >1000 >1000 233 3 1
norm. circRNA count
ε=0.9 ε=20.8 ε=408.9 ε=1590.8
total RNA Uninf. (WT)
total RNA 2h p.i. (WT)
total RNA 4h p.i. (WT)
total RNA 6h p.i. (WT)
total RNA 8h p.i. (WT)
c
n_h= 185 0 6 1
norm. circRNA count
ε=96.5 ε=21.1 ε=50.2
chrom.−asso. (uninf.)
chrom.−asso. (WT)
chrom.−asso. (ΔICP27)
chrom.−asso. (Δ*vhs*)
d
n_h= NA NA NA NA 512 71 32 7 3
norm. circRNA count
ε=1 ε=1 ε=1 ε=2.9 ε=6.4 ε=8.8 ε=33.4 ε=108.1
4sU−RNA Uninf. (Δ*vhs*)
4sU−RNA 0−1h p.i. (Δ*vhs*)
4sU−RNA 1−2h p.i. (Δ*vhs*)
4sU−RNA 2−3h p.i. (Δ*vhs*)
4sU−RNA 3−4h p.i. (Δ*vhs*)
4sU−RNA 4−5h p.i. (Δ*vhs*)
4sU−RNA 5−6h p.i. (Δ*vhs*)
4sU−RNA 6−7h p.i. (Δ*vhs*)
4sU−RNA 7−8h p.i. (Δ*vhs*)
e
n_h= >1000 >1000 >1000 26 5
norm. circRNA count
ε=0.7 ε=0.9 ε=14.3 ε=45.2
total RNA Uninf. (Δ*vhs*)
total RNA 2h p.i. (Δ*vhs*)
total RNA 4h p.i. (Δ*vhs*)
total RNA 6h p.i. (Δ*vhs*)
total RNA 8h p.i. (Δ*vhs*)
f
n_h= NA >1000 NA NA
norm. circRNA count
ε=5.7 ε=1 ε=1
cytos. (uninf.)
cytos. (WT)
cytos. (ΔICP27)
cytos. (Δ*vhs*)

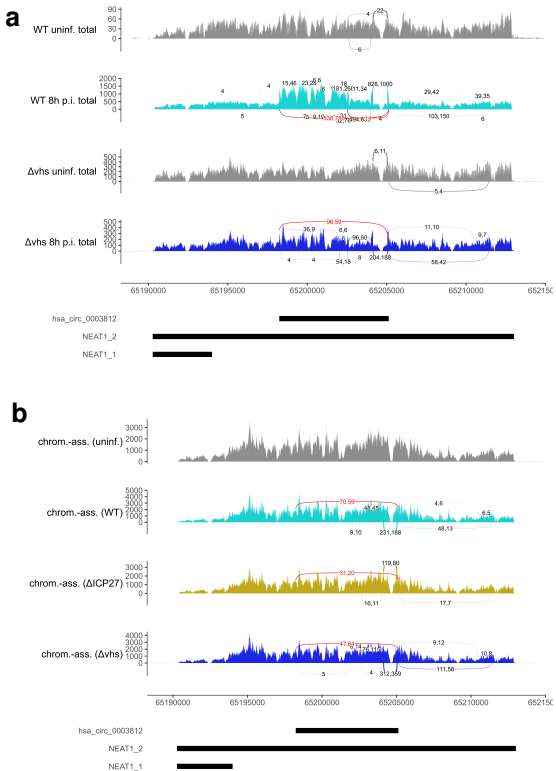
a
WT uninf. total
WT 8h p.i. total
Δvhs uninf. total
Δvhs 8h p.i. total
65190000
65195000
65200000
65205000
65210000
hsa_circ_0003812
NEAT1_2
NEAT1_1
b
chrom.-ass. (uninf.)
chrom.-ass. (WT)
chrom.-ass. (ΔICP27)
chrom.-ass. (Δvhs)
65190000
65195000
65200000
65205000
65210000
hsa_circ_0003812
NEAT1_2
NEAT1_1

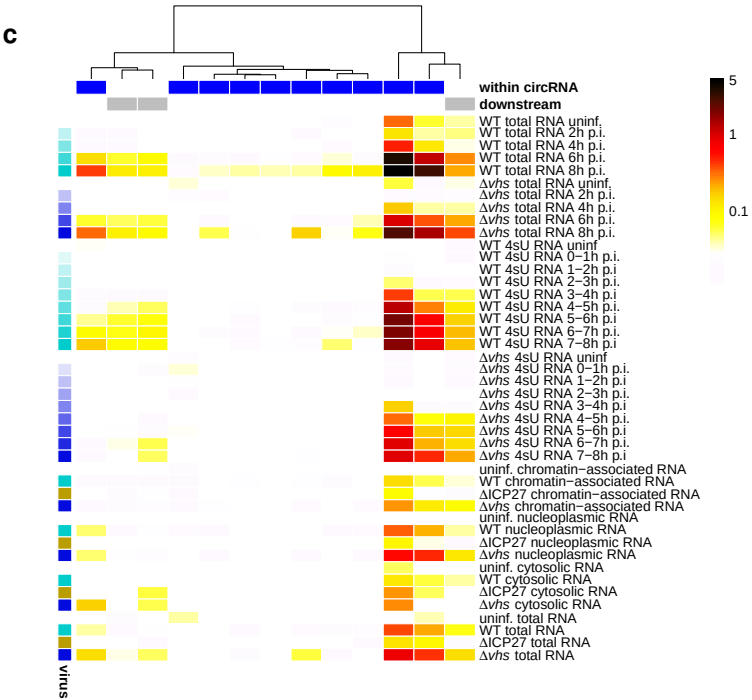
c
within circRNA
downstream
WT total RNA uninf.
WT total RNA 2h p.i.
WT total RNA 4h p.i.
WT total RNA 6h p.i.
WT total RNA 8h p.i.
Δvhs total RNA uninf.
Δvhs total RNA 2h p.i.
Δvhs total RNA 4h p.i.
Δvhs total RNA 6h p.i.
Δvhs total RNA 8h p.i.
WT 4sU RNA uninf
WT 4sU RNA 0−1h p.i.
WT 4sU RNA 1−2h p.i
WT 4sU RNA 2−3h p.i.
WT 4sU RNA 3−4h p.i
WT 4sU RNA 4−5h p.i.
WT 4sU RNA 5−6h p.i
WT 4sU RNA 6−7h p.i.
WT 4sU RNA 7−8h p.i
Δvhs 4sU RNA uninf
Δvhs 4sU RNA 0−1h p.i.
Δvhs 4sU RNA 1−2h p.i
Δvhs 4sU RNA 2−3h p.i.
Δvhs 4sU RNA 3−4h p.i
Δvhs 4sU RNA 4−5h p.i.
Δvhs 4sU RNA 5−6h p.i
Δvhs 4sU RNA 6−7h p.i.
Δvhs 4sU RNA 7−8h p.i
uninf. chromatin−associated RNA
WT chromatin−associated RNA
ΔICP27 chromatin−associated RNA
Δvhs chromatin−associated RNA
uninf. nucleoplasmic RNA
WT nucleoplasmic RNA
ΔICP27 nucleoplasmic RNA
Δvhs nucleoplasmic RNA
uninf. cytosolic RNA
WT cytosolic RNA
ΔICP27 cytosolic RNA
Δvhs cytosolic RNA
uninf. total RNA
WT total RNA
ΔICP27 total RNA
Δvhs total RNA
virus
5
1
0.1

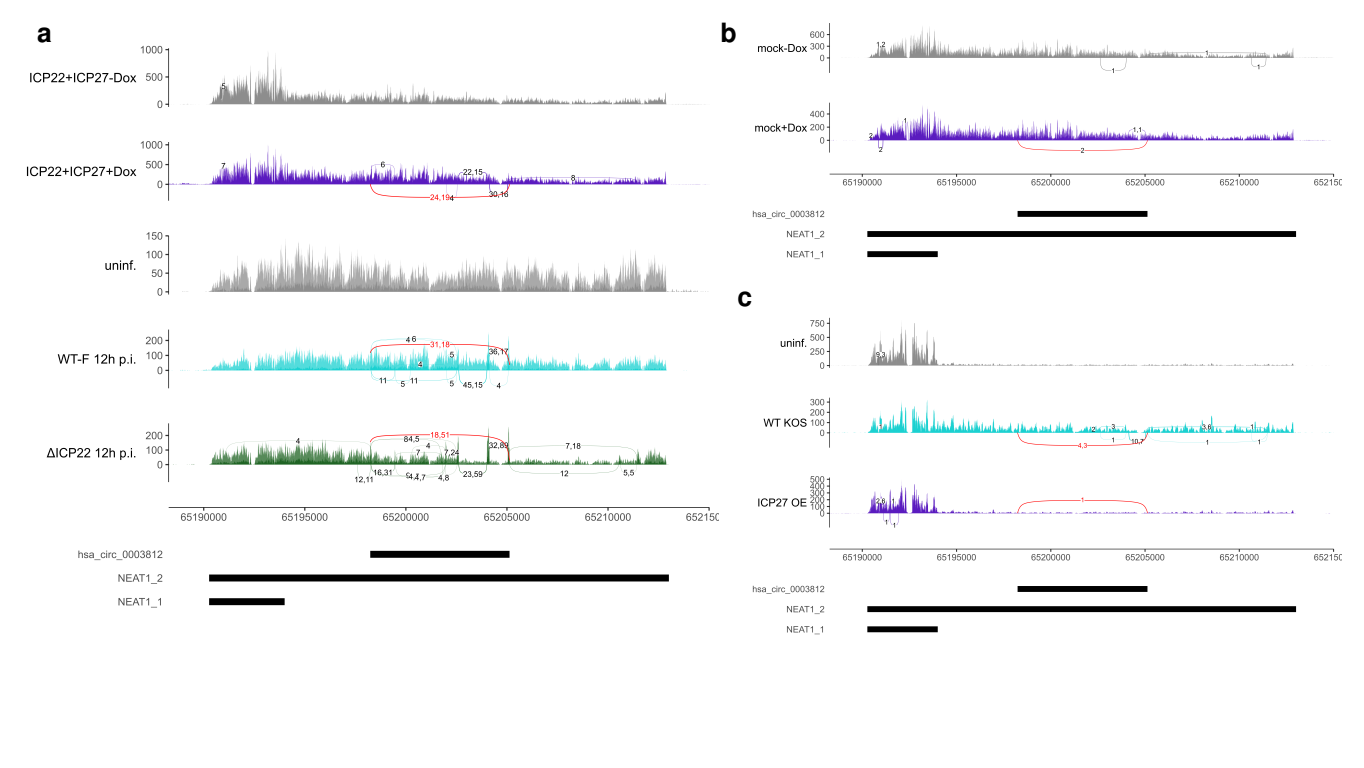
a
ICP22+ICP27-Dox
ICP22+ICP27+Dox
uninf.
WT-F 12h p.i.
ΔICP22 12h p.i.
hsa_circ_0003812
NEAT1_2
NEAT1_1
b
mock-Dox
mock+Dox
c
uninf.
WT KOS
ICP27 OE
65190000
65195000
65200000
65205000
65210000

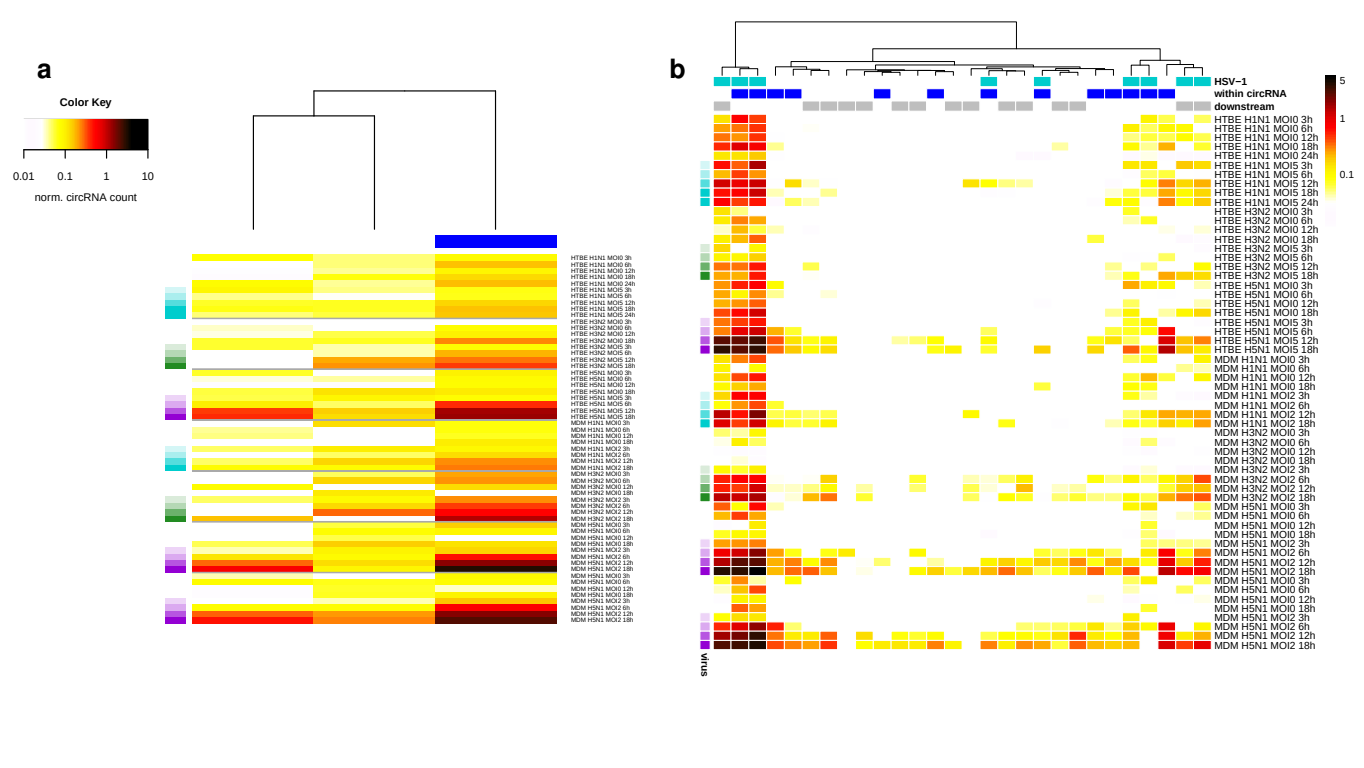
a
Color Key
0.01
0.1
1
10
norm. circRNA count
HTBE H1N1 MOI0 3h
HTBE H1N1 MOI0 6h
HTBE H1N1 MOI0 12h
HTBE H1N1 MOI0 18h
HTBE H1N1 MOI0 24h
HTBE H1N1 MOI5 3h
HTBE H1N1 MOI5 6h
HTBE H1N1 MOI5 12h
HTBE H1N1 MOI5 18h
HTBE H1N1 MOI5 24h
HTBE H3N2 MOI0 3h
HTBE H3N2 MOI0 6h
HTBE H3N2 MOI0 12h
HTBE H3N2 MOI0 18h
HTBE H3N2 MOI5 3h
HTBE H3N2 MOI5 6h
HTBE H3N2 MOI5 12h
HTBE H3N2 MOI5 18h
HTBE H5N1 MOI0 3h
HTBE H5N1 MOI0 6h
HTBE H5N1 MOI0 12h
HTBE H5N1 MOI0 18h
HTBE H5N1 MOI5 3h
HTBE H5N1 MOI5 6h
HTBE H5N1 MOI5 12h
HTBE H5N1 MOI5 18h
MDM H1N1 MOI0 3h
MDM H1N1 MOI0 6h
MDM H1N1 MOI0 12h
MDM H1N1 MOI0 18h
MDM H1N1 MOI2 3h
MDM H1N1 MOI2 6h
MDM H1N1 MOI2 12h
MDM H1N1 MOI2 18h
MDM H3N2 MOI0 3h
MDM H3N2 MOI0 6h
MDM H3N2 MOI0 12h
MDM H3N2 MOI0 18h
MDM H3N2 MOI2 3h
MDM H3N2 MOI2 6h
MDM H3N2 MOI2 12h
MDM H3N2 MOI2 18h
MDM H5N1 MOI0 3h
MDM H5N1 MOI0 6h
MDM H5N1 MOI0 12h
MDM H5N1 MOI0 18h
MDM H5N1 MOI2 3h
MDM H5N1 MOI2 6h
MDM H5N1 MOI2 12h
MDM H5N1 MOI2 18h
b
HSV−1
within circRNA
downstream
virus
5
1
0.1

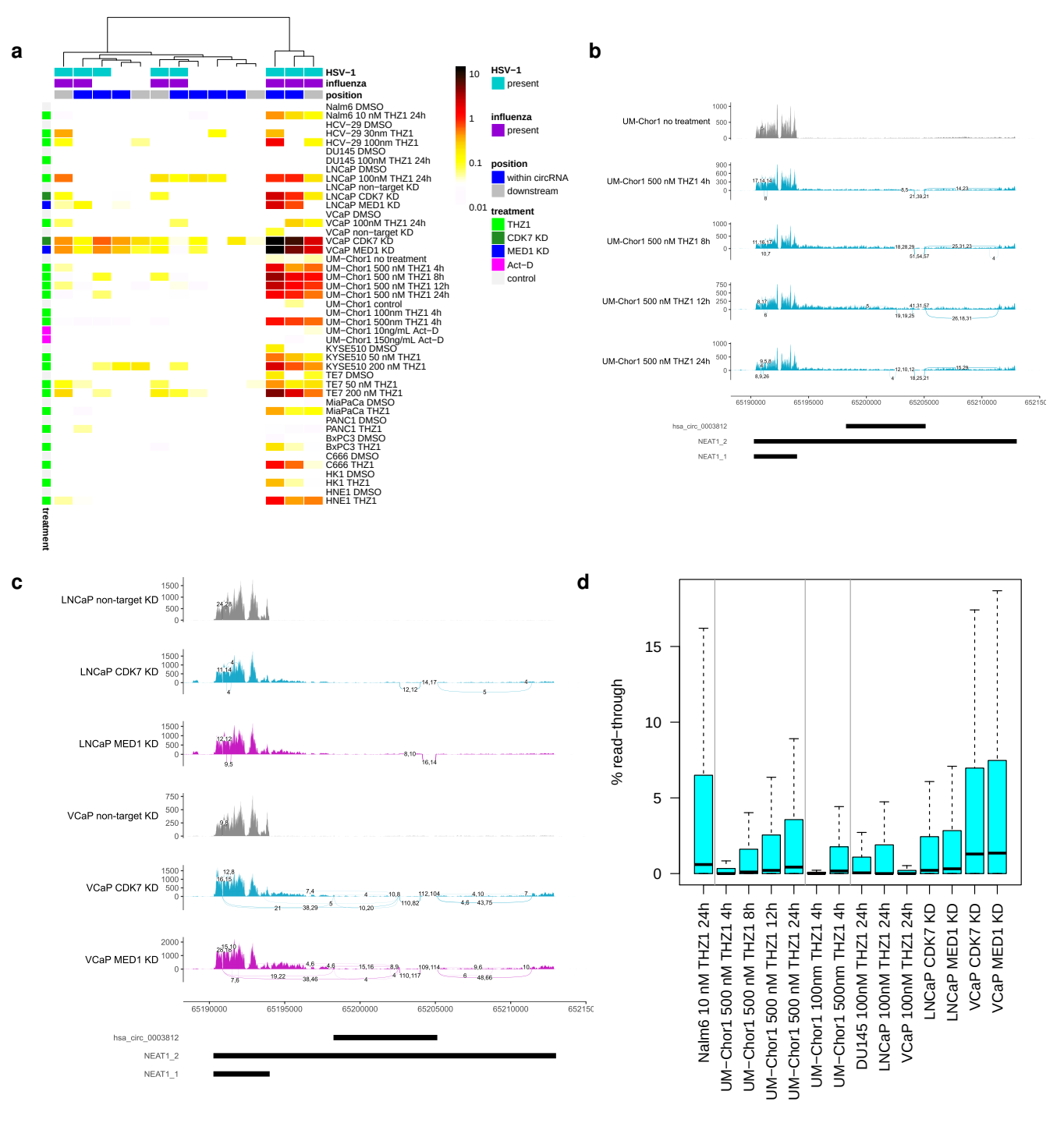
a
HSV−1
influenza
position
treatment
Nalm6 DMSO
Nalm6 10 nM THZ1 24h
HCV−29 DMSO
HCV−29 30nm THZ1
HCV−29 100nm THZ1
DU145 DMSO
DU145 100nM THZ1 24h
LNCaP DMSO
LNCaP 100nM THZ1 24h
LNCaP non−target KD
LNCaP CDK7 KD
LNCaP MED1 KD
VCaP DMSO
VCaP 100nM THZ1 24h
VCaP non−target KD
VCaP CDK7 KD
VCaP MED1 KD
UM−Chor1 no treatment
UM−Chor1 500 nM THZ1 4h
UM−Chor1 500 nM THZ1 8h
UM−Chor1 500 nM THZ1 12h
UM−Chor1 500 nM THZ1 24h
UM−Chor1 control
UM−Chor1 100nm THZ1 4h
UM−Chor1 500nm THZ1 4h
UM−Chor1 10ng/mL Act−D
UM−Chor1 150ng/mL Act−D
KYSE510 DMSO
KYSE510 50 nM THZ1
KYSE510 200 nM THZ1
TE7 DMSO
TE7 50 nM THZ1
TE7 200 nM THZ1
MiaPaCa DMSO
MiaPaCa THZ1
PANC1 DMSO
PANC1 THZ1
BxPC3 DMSO
BxPC3 THZ1
C666 DMSO
C666 THZ1
HK1 DMSO
HK1 THZ1
HNE1 DMSO
HNE1 THZ1
10
1
0.1
0.01
HSV−1
present
influenza
present
position
within circRNA
downstream
treatment
THZ1
CDK7 KD
MED1 KD
Act−D
control
b
UM-Chor1 no treatment
UM-Chor1 500 nM THZ1 4h
UM-Chor1 500 nM THZ1 8h
UM-Chor1 500 nM THZ1 12h
UM-Chor1 500 nM THZ1 24h
65190000
65195000
65200000
65205000
65210000
hsa_circ_0003812
NEAT1_2
NEAT1_1
c
LNCaP non-target KD
LNCaP CDK7 KD
LNCaP MED1 KD
VCaP non-target KD
VCaP CDK7 KD
VCaP MED1 KD
65190000
65195000
65200000
65205000
65210000
hsa_circ_0003812
NEAT1_2
NEAT1_1
d
% read−through
Nalm6 10 nM THZ1 24h
UM−Chor1 500 nM THZ1 4h
UM−Chor1 500 nM THZ1 8h
UM−Chor1 500 nM THZ1 12h
UM−Chor1 500 nM THZ1 24h
UM−Chor1 100nm THZ1 4h
UM−Chor1 500nm THZ1 4h
DU145 100nM THZ1 24h
LNCaP 100nM THZ1 24h
VCaP 100nM THZ1 24h
LNCaP CDK7 KD
LNCaP MED1 KD
VCaP CDK7 KD
VCaP MED1 KD